Proton acceleration from a cryogenic hydrogen ribbon

Contact: p.martin@qub.ac.uk

P. Martin, S. Kar,
D. Margarone, M. Borghesi
Centre for Plasma Physics,
Queen's University Belfast,
United Kingdom

H. Ahmed, D. Carroll
Central Laser Facility,
Rutherford Appleton Laboratory,
United Kingdom

D. Doria
ELI NP,
Magurele, Ilfov,
Romania

A. Alejo
Department of Physics,
University of Oxford,
United Kingdom

P. Bonnay, D. Chatain, D. Garcia,
S. Michaux, J. P. Perin
CEA,
Grenoble,
France

F. Grepl, L. Guiffrida, P. Lutoslawski,
F. Schillaci, V. Scuderi, A. Velyhan
ELI Beamlines,
Dolní Břežany,
Czechia

Abstract

Presented here are the results of an experimental campaign undertaken on the Petawatt arm of the Vulcan laser system in the Central Laser Facility in the UK. In the experiment thin (75–100μm) ribbons of cryogenically cooled solid hydrogen was used as a target. The interaction of a picosecond pulse with an intensity on the order of 10^{20} W/cm^2 produced beams of protons which are compared to results obtained with plastic flat foil targets. In addition to broadband TNSA-like spectra seen in both target types, quasi-monoenergetic bunching is observed at energies exceeding the TNSA cutoff for the cryogenic hydrogen targets, directed predominantly along the laser axis, suggesting a significant radiation pressure contribution to the acceleration dynamics. 2D particle-in-cell simulations are also presented, which demonstrate a strong relativistic self-focusing and channelling of the pulse inside the target, enhancing proton energies via the hole boring mechanism. These enhanced hole boring protons are suggested as a possible source for the experimentally observed quasi-monoenergetic peaks.

1 Introduction

In almost all applications of MeV ions, a pure beam with no contaminants is ideal. However, in most current laser-driven acceleration schemes, either due to the multispecies nature of most targets, or to the presence of hydrocarbon surface contaminants, the beams produced will contain several different elements in various ionisation states, which could need to be filtered out before the beam can be used. A target composed of pure hydrogen, therefore, is an ideal candidate for proton acceleration for this reason. However, hydrogen gas jets historically have seen limited use, due to their standard operating density being underdense for the most powerful lasers available today, which operate in the near-infrared (λ = 0.8-1μm). Using hydrogen cryogenically cooled to a solid state would alleviate this problem. Such a scheme was first employed by Saunders *et al.* in 1967 [1], achieving energies of several hundred eV from a 500MW ruby laser. In recent years, new cryogenic target delivery systems have been developed for use in laser applications. The cryogenic system used in this article was tested at two facilities, first at the kJ, nanosecond PALS facility, where a stream of protons with an energy up to 1 MeV was generated [2], and later at the short pulse ELFIE laser at LULI, where a maximum energy of 14MeV was demonstrated by Kraft *et al.* [3]. Recently, Obst *et al.* [4], using the Draco laser system, delivered an intensity of 6×10^{20}W/cm^2 with 30fs pulses and 3J on target energy, to accelerate protons via target normal sheath acceleration (TNSA) up to 20MeV from a solid/liquid hydrogen jet, produced form a different target delivery system than the one used in this campaign.

Another potential benefit of solid hydrogen over traditional solid targets (plastic or metal) is its much lower density. Solid hydrogen has an electron density of $\sim$54n$_c$, where n$_c$ is the critical density for laser light of 1.054μm wavelength (1.01×10^{21}cm^{-3}). This is around an order of magnitude lower than that of plastic (350n$_c$), which is a commonly used target in laser-driven ion acceleration. The lower density of solid hydrogen could improve the ion acceleration via radiation pressure acceleration (RPA), specifically the thick target regime known as hole boring (HB-RPA) [5]. The energy of ions accelerated via HB-RPA scales as $\varepsilon_{\max} \propto \Pi$ in the non-relativistic regime. The hole boring parameter, Π, is defined as $\Pi = \frac{I_0}{\rho c^3}$, where I$_0$ is the peak intensity, ρ is the density, and c is the speed of light in vacuum. Therefore, the pro-

ton energy accelerated by HB-RPA would be expected to be an order of magnitude higher with solid hydrogen than with plastic. This can be identified in the proton spectra by deviations from the typical broadband exponential TNSA spectrum.

2 Setup

The cryogenic target delivery system employed in this experiment, named ELISE, is described in [2] and [6]. With it, thin (75-100μm) planar ribbons of solid hydrogen could be produced. In addition, 9μm thick plastic (CH) flat foil targets were also shot, to serve as a reference. This thickness was chosen so that the CH targets had roughly the same areal density as the cryogenic target.

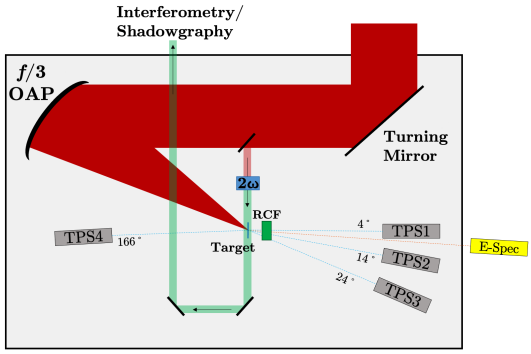

Figure 1: Schematic of the experimental arrangement in Vulcan.

The experiment was undertaken on the petawatt arm of the Vulcan laser system, at the Central Laser Facility in the UK. Here, pulses of ∼750fs duration and 300J of energy on target were focused at an angle of 15-20° to a spot with ∼5μm FWHM diameter, producing a peak intensity approaching 5×10^{20}W/cm^2. Ion diagnostics used were radiochromic film (RCF), and several Thomson parabola spectrometers (TPS) situated at 4°, 14°, 24°, and 166° relative to target normal, with Fujifilm BAS-TR imaging plates (IP) used as the detector. A schematic of the experimental setup is shown in Figure 1.

3 Results

All target spectra exhibited the broadband, Maxwell-Boltzmann spectrum typical of TNSA, however in the hydrogen targets there was a significant number of shots that featured a quasi-monoenergetic bunch at high energy, i.e. after the TNSA cutoff. Most of these features appeared in TPS3, corresponding to the direction of laser propagation, although two high energy peaks appeared on TPS1, target normal. No such proton bunching was seen for plastic targets. A selection of proton spectra from the TPS along target normal and laser axis for some

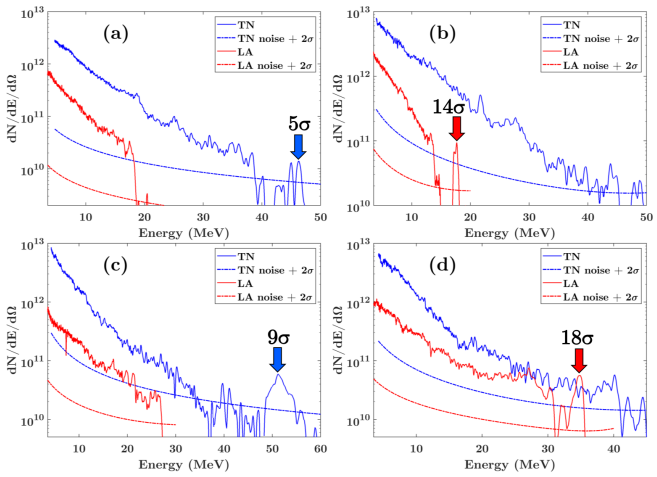

Figure 2: Proton spectra and the detection threshold taken along the **target normal** (TN) and **laser axis** (LA) TPS for solid hydrogen targets of (a) 75μm and (b,c,d) 100μm thickness. Quasi-monoenergetic bunches at high energy are indicated by the arrows, seen along target normal in (a) and (c), and laser axis in (b) and (d). The dip in the peak in (a) is due to a dead pixel on the IP. The statistical heights of each peak above the noise level are displayed on the plots.

hydrogen targets that feature the monoenergetic bunches is shown in Figure 2. The arrows indicate the peaks of these bunches, each of which are detected at statistical certainties above at least 5 standard devaitions. The measured statistical significance of each peak is shown above the arrows on the graph. The very high significance of these peaks shows that they are indeed real features, and are not the products of random noise fluctuations. Of the shots on hydrogen, ∼50% of shots show bunching, with a mean central energy of 34 ± 10MeV, with a mean energy spread ($\Delta E/E$) of 7%. The highest energy bunch (Figure 2(c)) produced in the experiment had a central energy of 52MeV, with the RCF stack detecting protons up to 60MeV (see Figure 3). This represents the highest energy produced to date from a cryogenic hydrogen target.

Bunches indictate acceleration mechanisms beyond TNSA. Additionally, the direction in which these bunches are detected can give us further insight into the dynamics. The bunches, for the most part, were detected along the laser axis, with a few exceptions directed along target normal, and not seen in multiple TPS in a single shot. This could indicate that the mechanism responsible for the bunching operates in only a narrow angular range. For ions accelerated from the front surface by HB-RPA from an obliquely incident laser, conservation of momentum dictates that the ions will be accelerated in the direction of target normal. However, if the laser pulse channels into the target, as has been observed in near critical targets in the past [7–11], then the hole bor-

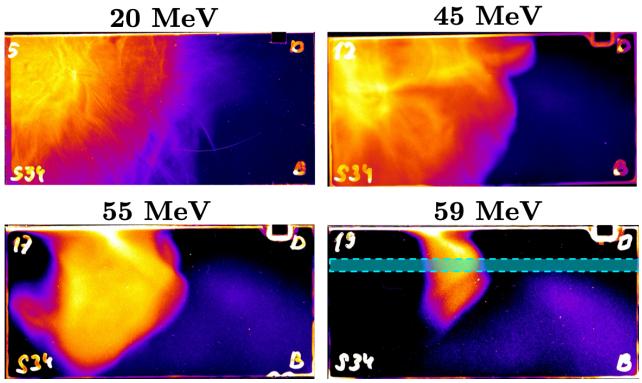

Figure 3: Selected RCF layers from the shot in Figure 4(a). The pixel values of the scanned RCF images have been converted to optical density, and the contrast of each layer individually adjusted to visually enhance features in the proton signal. Protons were visible up to the layer corresponding to 59MeV. All layers shown are of type EBT3. The cyan highlighted region indicates where the dose profile was taken in every layer.

ing front will travel in a direction close to the laser axis. This would present itself as a distinct beamlet of front accelerated protons diverging from the beam of rear surface protons accelerated via TNSA, separated approximately by the angle of incidence of the laser pulse ($\sim 20°$). This would be visible in the transverse beam profiles derived from the RCF stacks. To confirm this, proton dose profiles were taken from stacks from two shots on hydrogen, and one from a plastic target taken immediately after. The cyan coloured area in Figure 3 highlights the area in each layer the dose profile was taken.

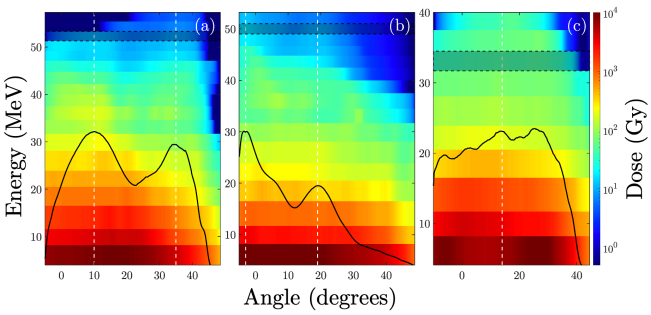

Figure 4: Dose profiles at all energies in an RCF stack with angle, for three consecutive shots on (a,b) 100μm hydrogen and (c) 9μm CH. The black solid lines are a lineout of the dose profile (in arbitrary units) across a high energy layer in each stack, indicated as the shaded area. White dashed lines denote the centre of the beamlets seen in the profiles. Angles on the x-axis are not with respect to target normal.

The dose profiles are shown in Figure 4. For the two shots on hydrogen, two distinct beamlets can be seen propagating $\sim 20°$ apart, approximately equal to the angular difference between target normal (leftmost dashed line) and the laser axis (rightmost dashed line). Lineouts of the dose profile across a high energy layer (indicated by the shaded rectangle) are overplotted on each graph, clearly showing the two beamlets for the HR targets. The profile of the CH target has a more uniform shape, showing a single symmetrical beam centred on target normal, as expected from a typical TNSA process. This provides further evidence that the protons from hydrogen ribbons are likely accelerated by two mechanisms competing for dominance, TNSA and HB-RPA, with the latter accelerating mainly along the direction of laser propagation, which can be caused by the laser pulse channelling inside the target. The RPA protons, originating from the front of the target, could also experience an enhanced post acceleration by the TNSA sheath field provided they are of high enough energy to reach the rear side of the target before the field has diminished.

4 Simulations

To support the experimental results, a series of 2D PIC simulations were run on the fully relativistic code EPOCH [12]. Due to constraints on the size of the simulation, the full 100μm target could not be simulated. This parameter in the simulations was therefore scaled down to a smaller value of 20μm,, while keeping all other variables true to experiment. The proton energies from TNSA would be higher with this thinner target geometry, although it was thick enough to not change by a significant amount with a picosecond duration pulse [13]. This allowed for a minimising of the load on the computing cluster, while keeping the conditions as close to reality as possible. A box 90μm wide in x and 65μm in y, with resolution $\Delta x \times \Delta y = (20 \times 20)\text{nm}^2$ was defined. Open boundaries were set for all x and y, with the laser source attached to the minimum x boundary. The target was initialised with an electron density of 54n_c[2], and a neutralising density of protons was input. All particles had an initial temperature of 1keV.

The laser pulse was p-polarised, and incident on the target surface at 20°, to match the experimental conditions. It had a Gaussian temporal profile with a duration (FWHM) of $\tau_p = 750$fs, with the total envelope $\sim 2\tau_p$ wide, encompassing 98% of the pulse energy. It was focused onto the target surface to a spot with a Gaussian profile 6μm in width (FWHM), reaching a peak intensity $\text{I}_0 = 5 \times 10^{20}\text{W/cm}^2$.

The laser was observed to exhibit strong self-focusing and channelling through the solid hydrogen target, Figure 5 shows the formation of the channel 300fs after the interation of the peak of the pulse with the target. A maximum intensity of approximately $2 \times 10^{21}\text{W/cm}^2$ is achieved at the point of strongest self focusing, and the beam waist is reduced to a minimum of $\sim 1\mu$m, on the order of the laser wavelength. Figure 5 (b) and (c) shows the electron and proton densities at the same time. The

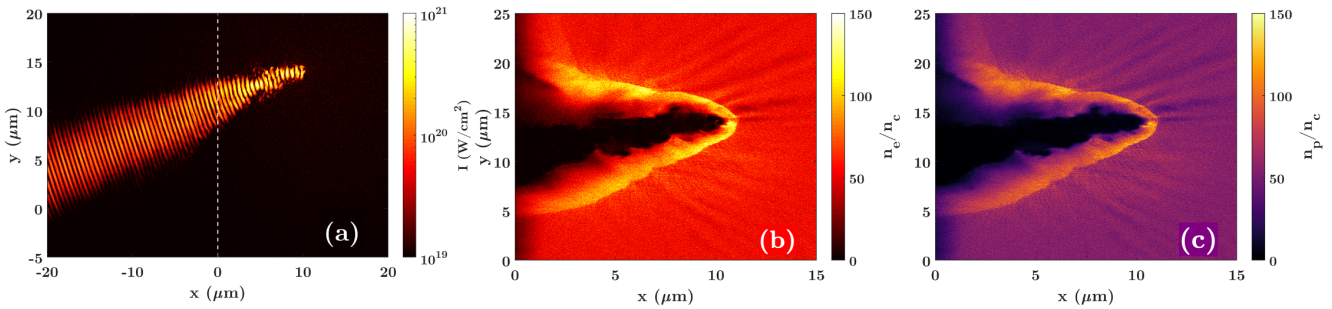

Figure 5: Results from a 2D PIC simualtion at a time 300fs after the incidence of the pulse peak at $x = 0\mu$m; showing (a) laser intensity, with strong channelling and self-focusing of the pulse visible. The dashed line indicates the initial position of the target front surface. (b) Electron, and (c) proton densities around the channel at the same time, normalised to the critical density, n_c.

pulse has completely cleared almost all particles from the channel, forming a low density cavity. This lower electron density of the channel, as well as the relativistic energies of the electrons accelerated by the laser field, results in ponderomotive [14] and relativistic [15] self-focusing.

The input intensity was varied in the simulation from $(1-10)\times 10^{20}$W/cm^2, and the HB proton energies were extracted and compared to a short pulse ($\tau_p = 40$fs) and what is expected analytically [16] (Figure 6). The short pulse laser does not exhibit channelling or self-focusing inside the target, and so the energies are found to agree with theory. The full scale pulse length shows a large deviation in the maximum energies from prediction, due to the self-focusing of the pulse to higher intensities. The red points are the same long pulse data, which have been rescaled to a laser intensity calculated from the peak cycle averaged electric field measured in the channel. This rescaling agrees well with what is predicted by theory. The unscaled data still scales quadratically with the a_0 (i.e. linearly with the intensity), implying that the strength of self-focusing, and the power dissipated inside the target, is not intensity dependent, at least in the range of intensities investigated. The self-focused intensity would be expected to be higher in 3 dimensions, due to the lower power that is dissipated by the pulse while in the channel in a higher dimensionality, as shown by Pukhov *et al.* [7]. This higher intensity from self-focusing in 3D could be the reason why the experimentally observed energies of the proton bunches were higher than what would be expected from the 2D PC simulations, which implied that the self-focused pulse, reaching an a_0 of ∼40, could only generate proton energies of ∼20MeV, 14MeV lower than the average energy detected.

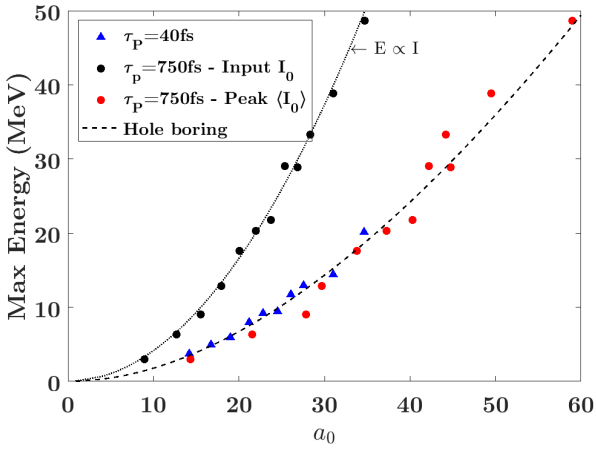

Figure 6: 2D PIC results, showing scaling of the maximum energy of protons accelerated by radiation pressure in solid hydrogen with the laser strength parameter, a_0. The results utilising two pulse lengths, 40fs and 750fs, are shown, with the 750fs data also rescaled to the higher a_0 calculated from the cycle-averaged peak electric field. The predicted maximum energy according to the analytical hole boring equations is denoted by the dashed line.

5 Conclusion

The highest recorded proton energies to date from a cryogenically cooled solid hydrogen target have been reported, reaching energies up to 60MeV. Additionally, quasi-monoenergetic bunches at central energies up to 52MeV were observed, indicating a strong influence on the acceleration from hole boring RPA. Two distinct beamlets, separated by the laser incidence angle, were seen in RCF for the hydrogen target, while plastic targets exhibited only a single beam. This corresponds to a beamlet accelerated by TNSA, and a beamlet accelerated along the laser propagation direction, further evidence of multiple acceleration mechanisms inside solid hydrogen, such as hole boring. The second proton beam being directed along the laser axis provides evidence, in most cases, of some pulse channelling inside the target, influencing the direction of the hole boring protons. 2D PIC

simulations have been presented, which show a significant channelling and self-focusing of the pulse inside the target, enhancing the energies of the hole boring protons and directing them primarily along the laser axis direction.

References

[1] P.A.H. Saunders, P. Avivi, and W. Millar. Laser produced plasmas from solid hydrogen targets. *Physics Letters A*, 24 (5):290 – 291, 1967. ISSN 0375-9601. doi: https://doi.org/10.1016/0375-9601(67)90443-4.

[2] D. Margarone, A. Velyhan, J. Dostal, J. Ullschmied, J. P. Perin, D. Chatain, S. Garcia, P. Bonnay, T. Pisarczyk, R. Dudzak, M. Rosinski, J. Krasa, L. Giuffrida, J. Prokupek, V. Scuderi, J. Psikal, M. Kucharik, M. De Marco, J. Cikhardt, E. Krousky, Z. Kalinowska, T. Chodukowski, G. A P Cirrone, and G. Korn. Proton acceleration driven by a nanosecond laser from a cryogenic thin solid-hydrogen ribbon. *Phys. Rev. X*, 6(4), 2016. ISSN 21603308. doi: 10.1103/PhysRevX.6.041030.

[3] Stephan D Kraft, Lieselotte Obst, Josefine Metzkes-Ng, Hans-Peter Schlenvoigt, Karl Zeil, Sylvain Michaux, Denis Chatain, Jean-Paul Perin, Sophia N Chen, Julien Fuchs, Maxence Gauthier, Thomas E Cowan, and Ulrich Schramm. First demonstration of multi-MeV proton acceleration from a cryogenic hydrogen ribbon target. *Plasma Physics and Controlled Fusion*, 60(4):044010, mar 2018. doi: 10.1088/1361-6587/aaae38.

[4] Lieselotte Obst, Sebastian Göde, Martin Rehwald, Florian Emanuel Brack, João Branco, Stefan Bock, Michael Bussmann, Thomas E. Cowan, Chandra B. Curry, Frederico Fiuza, Maxence Gauthier, René Gebhardt, Uwe Helbig, Axel Huebl, Uwe Hübner, Arie Irman, Lev Kazak, Jongjin B. Kim, Thomas Kluge, Stephan Kraft, Markus Loeser, Josefine Metzkes, Rohini Mishra, Christian Rödel, Hans Peter Schlenvoigt, Mathias Siebold, Josef Tiggesbäumker, Steffen Wolter, Tim Ziegler, Ulrich Schramm, Siegfried H. Glenzer, and Karl Zeil. Efficient laser-driven proton acceleration from cylindrical and planar cryogenic hydrogen jets. *Sci. Rep.*, 7(1), 2017. ISSN 20452322. doi: 10.1038/s41598-017-10589-3.

[5] Andrea Macchi. *A Superintense Laser-Plasma Interaction Theory Primer*. 2013. ISBN 9789400761247. doi: 10.1007/978-94-007-6125-4.

[6] S. Garcia, D. Chatain, and J. P. Perin. Continuous production of a thin ribbon of solid hydrogen. *Laser Part. Beams*, 760:569–575, 2014. ISSN 1469803X. doi: 10.1017/S0263034614000524.

[7] A Pukhov and J Meyer-ter Vehn. Relativistic magnetic self-channeling of light in plasma. Three-dimensional PIC simulation. *Phys. Rev. Lett.*, 76:3975–3978, 1996.

[8] A. Pukhov and J. Meyer-Ter-Vehn. Laser Hole Boring into Overdense Plasma and Relativistic Electron Currents for Fast Ignition of ICF Targets. *Phys. Rev. Lett.*, 79(14):2686–2689, 1997. ISSN 10797114. doi: 10.1103/PhysRevLett.79.2686.

[9] M. Borghesi, A. J. MacKinnon, L. Barringer, R. Gaillard, L. A. Gizzi, C. Meyer, O. Willi, A. Pukhov, and J. Meyer-Ter-Vehn. Relativistic Channeling of a Picosecond Laser Pulse in a Near-Critical Preformed Plasma. *Phys. Rev. Lett.*, 78(5): 879–882, 1997. ISSN 10797114. doi: 10.1103/PhysRevLett.78.879.

[10] Baifei Shen and M. Y. Yu. Relativistic channeling by intense laser pulse in overdense plasmas. *Phys. Rev. E - Stat. Physics, Plasmas, Fluids, Relat. Interdiscip. Top.*, 68(2):4, 2003. ISSN 1063651X. doi: 10.1103/PhysRevE.68.026501.

[11] A. L. Lei, A. Pukhov, R. Kodama, T. Yabuuchi, K. Adumi, K. Endo, R. R. Freeman, H. Habara, Y. Kitagawa, K. Kondo, G. R. Kumar, T. Matsuoka, K. Mima, H. Nagatomo, T. Norimatsu, O. Shorokhov, R. Snavely, X. Q. Yang, J. Zheng, and K. A. Tanaka. Relativistic laser channeling in plasmas for fast ignition. *Phys. Rev. E - Stat. Nonlinear, Soft Matter Phys.*, 76(6):1–5, 2007. ISSN 15393755. doi: 10.1103/PhysRevE.76.066403.

[12] T. D. Arber, K. Bennett, C. S. Brady, A. Lawrence-Douglas, M. G. Ramsay, N. J. Sircombe, P. Gillies, R. G. Evans, H. Schmitz, A. R. Bell, and C. P. Ridgers. Contemporary particle-in-cell approach to laser-plasma modelling. *Plasma Phys. Control. Fusion*, 57(11), 2015. ISSN 13616587. doi: 10.1088/0741-3335/57/11/113001.

[13] P. L. Poole, L. Obst, G. E. Cochran, J. Metzkes, H. P. Schlenvoigt, I. Prencipe, T. Kluge, T. Cowan, U. Schramm, D. W. Schumacher, and K. Zeil. Laser-driven ion acceleration via target normal sheath acceleration in the relativistic transparency regime. *New J. Phys.*, 20(1), 2018. ISSN 13672630. doi: 10.1088/1367-2630/aa9d47.

[14] Claire Ellen Max, Jonathan Arons, and A. Bruce Langdon. Self-modulation and self-focusing of electromagnetic waves in plasmas. *Phys. Rev. Lett.*, 33(4):209–212, 1974. ISSN 00319007. doi: 10.1103/PhysRevLett.33.209.

[15] Burke Ritchie. Relativistic self-focusing and channel formation in laser-plasma interactions. *Phys. Rev. E*, 50(2):687–689, 1994. ISSN 1063651X. doi: 10.1103/PhysRevE.50.R687.

[16] Andrea Macchi, Federica Cattani, Tatiana V. Liseykina, and Fulvio Cornolti. Laser acceleration of ion bunches at the front surface of overdense plasmas. *Phys. Rev. Lett.*, 94(16):2–5, 2005. ISSN 00319007. doi: 10.1103/PhysRevLett.94.165003.